JOURNAL OF GUIDANCE, CONTROL, AND DYNAMICS
Vol. 31, No. 1, January–February 2008

Optimal Crosswind Towing and Power Generation with Tethered Kites

Paul Williams,* Bas Lansdorp,† and Wubbo Ockels‡
Delft University of Technology, 2600 GB Delft, The Netherlands

DOI: 10.2514/1.30089

Nonpowered aerial vehicles such as kites can provide a means of transmitting wind energy from higher altitudes to the ground via tethers. Although there have been many proposals for systems to extract wind energy from higher altitudes, this paper focuses on the use of a light lifting body at the end of a tether to generate useful power. Two major configurations are studied: 1) the kite is used to tow a ground vehicle in the crosswind direction and 2) the kite is flown to generate power using a ground generator. In both cases, the useful work done by the kite is transmitted to the ground through the tether. Both applications require control of the kite trajectories. A simplified system model is used to study the nature of the optimal trajectories of the system for different wind speeds and system parameters. Numerical results illustrate that optimal power generation is most sensitive to the cycle time, tether length, and wind speed. The power output for power generation, as well as the average towing velocity for the towing case, are roughly proportional to the cube of the wind speed.

I. Introduction

WIND is an important source of energy. Over the last several decades, many proposals have been put forward for devices to extract and use wind energy. The most popular design concept is the horizontal axis wind turbine, which is placed relatively close to the ground. However, it has long been known that the Earth's surface creates a boundary-layer-like effect on the wind so that the wind speed generally increases with altitude. In fact, it is possible for significant wind to be present at higher altitudes with little to no wind on the ground. This knowledge has spawned several radical ideas for wind power extraction. However, many of the basic principles of transmitting wind energy to the ground have been used since the early days of kite-flying, when kites were used for towing boats and wagons [1] or for lifting objects such as weather instrumentation [2]. In these applications, a kite is flown to produce a beneficial lifting or pulling force that is transmitted to an object at lower altitude via a tether. However, as pointed out by Carpenter [1,2], with the advent of manned aircraft, such devices are seldom used today. One of the major problems encountered in the early application of kites for towing vehicles was the lack of adequate feedback control to cope with changing and unsteady winds. Modern-day control techniques are capable of circumventing some of these problems, which have seen renewed interest in kite research.

One of the most promising applications of tethered kites is for providing a means of generating electricity. At the most basic level, if control of the kite motion can be achieved remotely, then it is possible to manipulate the tension in the tether by changing the forces on the kite. For example, to increase tension, the kite angle of attack can be increased, thereby increasing the lift on the kite. Conversely, to decrease tension, the kite angle of attack is decreased. Much more complex motions can be envisioned. The forces on the kite are a function of the kite angle of attack, its roll angle, and the local relative air speed. The most important of these for increasing the total lift force is the air speed, because doubling it results in a fourfold increase in lift. Therefore, ways of achieving higher relative air speeds is an important issue to be addressed. By controlling the forces on the kite, thereby influencing the cable tension, it is possible to generate net power by using a drum that is capable of paying the cable in and out. If the tether is let out at high tension, it is generating power. If the tether is then reeled back in, it is using power. The key idea is to control the kite in such a way that the tension during the reel-in phase is much lower than the tension during the payout phase. The larger the difference in tension during reel-in and reel-out, the greater the power that can be generated.

This paper investigates the optimal means for flying a kite to produce maximum power for the purposes of electricity generation, as well as for towing ground vehicles. These two applications are related by the fact that the tether is used to produce work on the ground. For power generation, the kite needs to be flown in a manner that produces alternate periods of high and low tension, at which time the tether must be reeled with similar phasing. For towing, the tension forces on the vehicle must directed in the towing direction with maximum tension throughout the motion. An alternative is to combine both power generation and towing, whereby power is generated on the vehicle to be used by an onboard propulsion system. However, this particular application of kite technology is not considered further in this work. The paper is structured as follows: first, a brief survey of concepts for high-altitude wind power is presented; next, the simplified dynamic model of the system that is used for the analysis is derived and compared with a more complex model of the tether; the optimal control problem(s) are defined and the numerical solution technique is described; results are presented for different operating conditions for both power generation and crosswind towing; and, finally, some conclusions are drawn.

II. Wind Energy Extraction from High Altitude

The fact that wind is relatively slow close to the ground has long been known. The Earth's surface creates a boundary-layer effect so that winds generally increase with altitude. Two wind profiles are often used to model the variation in wind close to the surface [3]:

$$V = (V^*/\kappa)[\ell_n(h/h_0) - \Psi(h/L^*)] \tag{1}$$

$$V = V_r(h/h_r)^\alpha \tag{2}$$

where V is the wind speed at altitude h, h_0 is a roughness length, κ is von Kármán's constant (0.4), $\Psi(h/L^*)$ is a correction for nonneutral

Received 29 January 2007; revision received 31 August 2007; accepted for publication 3 September 2007.

*Visiting Scholar, Unit 1, 4 Maylands Avenue, Balwyn North Victoria 3104; tethered.systems@gmail.com. Member AIAA.

†Ph.D. Researcher, Faculty of Aerospace Engineering, P.O. Box Postbus 5058; b.lansdorp@tudelft.nl.

‡ASSET Chairholder, Faculty of Aerospace Engineering, P.O. Box Postbus 5058; w.j.ockels@tudelft.nl.

stratification defined as a function of altitude and the Monin–Obukhov length L^* [4], the subscript r refers to some reference velocity and height, and α is the power-law index that varies as a function of surface friction (e.g., ~0.10 for smooth surfaces such as a lake or ocean and ~0.40 for an urban area with tall buildings) [5]. The reference height h_r typically varies between 10 and 100 m [3,6], depending on the location of the measurement equipment. In addition, the power-law index has been found to vary as a function of the surface wind speed [6]. Above a particular height h^*, the wind speed can be treated as constant [note that this does not necessarily correspond to h_r in Eq. (2) (i.e., $h^* > h_r$)] [6].

The idea of using airborne windmills for electricity generation was investigated at least as far back as the 1930s [7–9]. Riegler and Riedler [10], and Riegler et al. [11] proposed the idea of using a turbine wind generator mounted on a tethered balloon or aerostat. Fletcher and Roberts [7] and Roberts and Shepard [12] described the concept of a rotorcraft situated nearly permanently in the upper atmosphere for generating electricity. Their design uses an airframe with two or more identical rotors inclined at a controlled angle to the wind stream. The rotors are designed to generate electricity as well as to provide lift to support the airframe. Fletcher [13] discussed using a system consisting of a platform with rotary wings to provide power from the jet stream, but concluded that it would have very high operating costs because of the need to replace the key components frequently. Furthermore, Rye [14] performed a linear stability analysis of the tethered rotorcraft and found that the system is stable for short tether lengths, but unstable for long cables. A number of other concepts for extracting wind energy through tethered systems at high altitudes have also been proposed. Many of these concepts also propose to locate the electric generator at altitude [15,16].

One of the major drawbacks of the aforementioned systems is that the power generator is collocated with the wind energy source. This means that the system must support a significant load in addition to the cable loads. This raises some problems in launching the system to the desired altitude and, more significantly, introduces additional costs. An alternative concept called the laddermill was proposed by Ockels [17], in which power is generated by a series of high-lifting wings or kites that move a cable through an electric generator. The closed cable consists of an upside and downside. The wings on the upside operate at high angles of attack, generating high lift and pulling the cable upward, whereas the wings on the downside generate very low lift. The difference in tension at the ground winch causes the cable to be pulled through the generator, generating electric power. Meijaard et al. [18] developed a mathematical model for the laddermill, including the effect of blade dynamics, and found that the blade rotation is unstable in the presence of disturbances. Lansdorp and Ockels [19] also suggested the idea of a pumping mill, which consists of a single cable with connected wings rather than a looped cable. It was concluded that the pumping mill is a simpler and lighter-weight option. Small-scale tests using a surf kite have been conducted with the kite motion controlled by drag flaps on the sides of the kite [20], as well as with sliding attachment points on the sides of the kite [21].

Loyd [22] suggested that a kite could be used to fly a closed-path downwind of a tether and transverse to the direction of the wind. The lift could be used to both support the kite and to generate power. He suggested either using the tether tension to "pull a load" or using an air turbine on the kite itself to generate power. Carpenter [2] suggested that rather than using a generator on the kite, the tether could be pulled off a drum that drives a rotor on the ground. The kite would be remotely controlled such that its angle of attack is manipulated as a function of position downwind.

Of all the proposals put forward for extracting high-altitude wind energy, the kite pumping mill appears to have the most promise due to its low costs and lighter weight relative to high-altitude turbine concepts. Hence, in the remainder of this paper, the tethered kite concept for generating power and crosswind towing is examined. In particular, a small-scale version of such a system is studied from the point of view of dynamics and control. Full-scale versions of the system might conceivably reach altitudes between 1–3 km and would likely consist of multiple kites rather than a single kite.

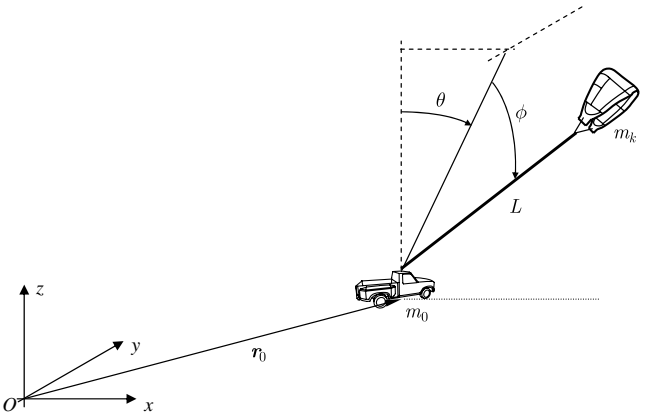

Fig. 1 Simplified representation of a tethered kite system with a moving ground vehicle.

III. Dynamic Modeling of a Tethered Kite System

A. Towing Case

The system is modeled as consisting of a kite connected to a ground vehicle. The dynamics are simplified to enable an efficient study of optimal kite trajectories. Thus, the ground vehicle and kite are modeled as a point mass, with the forces on the kite generated as functions of the angle of attack and roll angle. The tether is assumed to remain straight, but the effects of distributed mass and drag are considered. The validity of the assumption of a straight tether depends on the tension in the tether, its length, and its mass. Generally, the tether will take on a slightly curved shape due to the action of drag and gravity. The impact of this curvature is to alter the drag loading on the tether and shorten the distance between the winch and the tether tip. In dynamic simulations, changes in tether shape also lead to stringlike vibrations. These vibrations are ignored for the purposes of initial design, due to high aerodynamic damping.

The system model incorporating a moving ground vehicle is shown in Fig. 1. The position and velocity of the ground vehicle is specified by its Cartesian components $\boldsymbol{r}_0$ and $\dot{\boldsymbol{r}}_0$ in the inertial coordinate system $Oxyz$. The instantaneous mass of the ground vehicle is $m_0 = m_0^0 - \rho_c L$, where ρ_c is the density per unit length of the tether, and L is the length of the deployed tether. The position of the kite of mass m_k is represented using the spherical coordinates L, θ, and ϕ relative to the ground vehicle. The angle θ represents the angle of the tether to the vertical in the plane of the wind, whereas ϕ is the out-of-plane (crosswind) component. These definitions imply, without loss of generality, that the wind is nominally parallel to the x axis.

The equations of motion for the system are derived using Lagrange's equations. Consider an arbitrary point at a distance s along the tether measured from the ground vehicle toward the kite. The position vector of this point can be written as

$$\boldsymbol{r}(s) = \boldsymbol{r}_0 + s\cos\phi\sin\theta\boldsymbol{i} + s\sin\phi\boldsymbol{j} + s\cos\phi\cos\theta\boldsymbol{k} \tag{3}$$

The inertial velocity of the point s is given by

$$\begin{aligned}\dot{\boldsymbol{r}}(s) = {} & (\dot{x} + \dot{s}\cos\phi\sin\theta - s\dot{\phi}\sin\phi\sin\theta + s\dot{\theta}\cos\phi\cos\theta)\boldsymbol{i} \\ & + (\dot{y} + \dot{s}\sin\phi + s\dot{\phi}\cos\phi)\boldsymbol{j} \\ & + (\dot{z} + \dot{s}\cos\phi\cos\theta - s\dot{\phi}\cos\phi\cos\theta - s\dot{\theta}\cos\phi\cos\theta)\boldsymbol{k}\end{aligned} \tag{4}$$

The tether is assumed to be rigid and, hence, $\dot{s} = \dot{L}$. For a tether of uniform mass with line density ρ_c, the ground vehicle mass is a function of tether length according to $m_0 = m_0^0 - \rho_c L$. Thus, the kinetic energy of the system is given by

$$\begin{aligned}\mathcal{T} = {} & \frac{1}{2}m_0(\dot{x}^2 + \dot{y}^2 + \dot{z}^2) + \frac{1}{2}\rho_c\int_0^L \dot{\boldsymbol{r}}(s)\cdot\dot{\boldsymbol{r}}(s)\mathrm{d}s \\ & + \frac{1}{2}m_k\dot{\boldsymbol{r}}(s)\cdot\dot{\boldsymbol{r}}(s)|_{s=L}\end{aligned} \tag{5}$$

The potential energy of the system is given by

$$\mathcal{V} = m_0 g z + \rho_c L g z + m_k g z + \tfrac{1}{2}\rho_c g L^2 \cos\theta\cos\phi + m_k g L \cos\theta\cos\phi \tag{6}$$

The equations of motion are derived by direct application of Lagrange's equations in the form

$$\frac{\mathrm{d}}{\mathrm{d}t}\left(\frac{\partial \mathcal{L}}{\partial \dot{q}_j}\right) - \frac{\partial \mathcal{L}}{\partial q_j} = Q_{q_j} \tag{7}$$

However, before progressing to present the coupled equations of motion, several points need to be made. First, the ground height is assumed to be prescribed so that $\ddot{z}$ is a constraint on the motion; that is, no vehicle suspension is modeled. Thus, z is not a generalized coordinate. Second, the ground vehicle is acted on by rolling friction, which is dependent on the normal reaction of the vehicle on the ground as well as its speed. The normal reaction of the vehicle on the ground is also a function of the cable tension. Because the cable is modeled as inelastic, it is necessary to solve for the constraint force and normal force on the ground simultaneously. The complicating factor is that the vehicle acceleration is a function of the rolling friction forces and therefore the ground reaction.

Define the normal reaction of the ground on the vehicle as N_z. The rolling resistance forces are assumed to oppose the direction defined by the velocity vector of the ground vehicle, which is assumed to be always in motion. Assuming no slip, the rolling resistance of the vehicle can be defined as [23]

$$F_x^f = F_R \frac{\dot{x}}{\sqrt{\dot{x}^2+\dot{y}^2}}, \qquad F_y^f = F_R \frac{\dot{y}}{\sqrt{\dot{x}^2+\dot{y}^2}}$$
$$F_R = -\mu_0 N_z - \mu_1 N_z \frac{\sqrt{\dot{x}^2+\dot{y}^2}}{30} - \mu_2 N_z \frac{(\dot{x}^2+\dot{y}^2)^2}{30^4} \tag{8}$$

where $\mu_0, \ldots, \mu_2$, are rolling resistance coefficients that depend on tire pressure. These friction forces account for the dissipation of energy that occurs in nonrigid tires during rolling motion. Thus, we define the ground reaction N_z as an unknown constraint parameter, together with the tether tension T. The equations for the z and L coordinates are used to enable the simultaneous solution of all unknowns, including the system accelerations. The resulting set of differential algebraic equations are given by

$$[\boldsymbol{M}][\ddot{x}, \ddot{y}, N_z, \ddot{\theta}, \ddot{\phi}, T]^\top = \boldsymbol{b} \tag{9}$$

where

$$\begin{aligned} b_x = {} & F_x^0 + F_x^k + F_x^t - \rho\dot{L}^2\cos\phi\sin\theta - m_k\ddot{L}\cos\phi\sin\theta \\ & + \tfrac{1}{2}\rho_c L^2\dot{\phi}^2\cos\phi\sin\theta + \dot{\theta}\,\dot{\phi}\,\rho_c L^2\sin\phi\cos\theta \\ & + \tfrac{1}{2}\dot{\theta}^2\rho_c L^2\cos\phi\sin\theta + 2\rho_c L\dot{L}\,\dot{\phi}\sin\phi\sin\theta \\ & - 2\dot{\theta}\rho_c L\dot{L}\cos\phi\cos\theta - \rho_c L\ddot{L}\cos\phi\sin\theta \\ & + 2m_k\dot{L}\,\dot{\phi}\sin\phi\sin\theta - 2\dot{\theta}m_k\dot{L}\cos\phi\cos\theta \\ & + m_k L\dot{\phi}^2\cos\phi\sin\theta + 2\dot{\theta}\,\dot{\phi}\,m_k L\sin\phi\cos\theta \\ & + m_k L\dot{\theta}^2\cos\phi\sin\theta \end{aligned} \tag{11}$$

$$\begin{aligned} b_y = {} & F_y^0 + F_y^k + F_y^t\tfrac{1}{2}\rho_c L^2\sin\phi\dot{\phi}^2 - 2\dot{\phi}\rho_c L\dot{L}\cos\phi - \rho_c L\ddot{L}\sin\phi \\ & - \rho_c\dot{L}^2\sin\phi - m_k\ddot{L}\sin\phi - 2\dot{\phi}m_k\dot{L}\cos\phi + m_k L\dot{\phi}^2\sin\phi \end{aligned} \tag{12}$$

$$\begin{aligned} b_z = {} & F_z^k + F_z^t - m_k\ddot{z} - m_0^0\ddot{z} - m_0^0 g + \tfrac{1}{2}\rho_c L^2\dot{\phi}^2\cos\phi\cos\theta \\ & - \rho_c L^2\dot{\phi}\,\dot{\theta}\sin\phi\sin\theta + \tfrac{1}{2}\rho_c L^2\dot{\theta}^2\cos\phi\cos\theta \\ & + 2\rho_c L\dot{L}\,\dot{\phi}\sin\phi\cos\theta + 2\rho_c L\dot{L}\,\dot{\theta}\cos\phi\sin\theta \\ & - \rho_c L\ddot{L}\cos\phi\cos\theta + 2m_k\dot{L}\,\dot{\phi}\sin\phi\cos\theta \\ & - 2m_k L\dot{\phi}\,\dot{\theta}\sin\phi\sin\theta + 2m_k\dot{L}\,\dot{\theta}\cos\phi\sin\theta \\ & + m_k L\dot{\phi}^2\cos\phi\cos\theta + m_k L\dot{\theta}^2\cos\phi\cos\theta \\ & - m_k\ddot{L}\cos\phi\cos\theta - m_k g - \rho_c\dot{L}^2\cos\phi\cos\theta \end{aligned} \tag{13}$$

$$\begin{aligned} b_\theta = {} & Q_\theta^t + Q_\theta^k - \rho_c L^2\dot{L}\,\dot{\theta}\cos^2\phi + m_k L\ddot{z}\cos\phi\sin\theta \\ & + \tfrac{1}{2}\rho_c L^2\ddot{z}\cos\phi\sin\theta + \tfrac{2}{3}\rho_c L^3\dot{\theta}\,\dot{\phi}\cos\phi\sin\phi - 2m_k\dot{L}\,\dot{\theta}\cos^2\phi \\ & + 2m_k L^2\dot{\theta}\,\dot{\phi}\cos\phi\sin\phi + \tfrac{1}{2}\rho_c g L^2\cos\phi\sin\theta \\ & + m_k g L\cos\phi\sin\theta \end{aligned} \tag{14}$$

$$\begin{aligned} b_\phi = {} & Q_\phi^k + Q_\phi^t - \rho_c L^2\dot{L}\,\dot{\phi} - 2m_k L\dot{L}\,\dot{\phi} + m_k g L\sin\phi\cos\theta \\ & + \tfrac{1}{2}\rho_c g L^2\sin\phi\cos\theta + m_k L\ddot{z}\sin\phi\cos\theta + \tfrac{1}{2}\rho_c L^2\ddot{z}\sin\phi\cos\theta \\ & - \tfrac{1}{3}\rho_c L^3\dot{\theta}^2\cos\phi\sin\phi - m_k L^2\dot{\theta}^2\cos\phi\sin\phi \end{aligned} \tag{15}$$

$$\begin{aligned} b_L = {} & Q_L^k - \rho_c L\ddot{z}\cos\phi\cos\theta - \rho_c g L\cos\phi\cos\theta - m_k\ddot{L} - \tfrac{1}{2}\rho_c\dot{L}^2 \\ & - m_k g\cos\phi\cos\theta - m_k\ddot{z}\cos\phi\cos\theta - \rho_c L\ddot{L} + \tfrac{1}{2}\rho_c L^2\dot{\theta}^2\cos^2\phi \\ & + m_k L\dot{\theta}^2\cos^2\phi + \tfrac{1}{2}\rho_c L^2\dot{\phi}^2 + m_k L\dot{\phi}^2 \end{aligned} \tag{16}$$

$$M = \begin{bmatrix} m_0^0 + m_k & 0 & \frac{\tilde{F}_R\dot{x}}{\sqrt{\dot{x}^2+\dot{y}^2}} & \left(\frac{\rho_c L}{2}+m_k\right)L\cos\theta\cos\phi & -\left(\frac{\rho_c L}{2}+m_k\right)L\sin\theta\sin\phi & 0 \\ 0 & m_0^0 + m_k & \frac{\tilde{F}_R\dot{y}}{\sqrt{\dot{x}^2+\dot{y}^2}} & 0 & \left(\frac{\rho_c L}{2}+m_k\right)L\cos\phi & 0 \\ 0 & 0 & -1 & -\left(\frac{\rho_c L}{2}+m_k\right)L\sin\theta\cos\phi & -\left(\frac{\rho_c L}{2}+m_k\right)L\cos\theta\sin\phi & 0 \\ \left(\frac{\rho_c L}{2}+m_k\right)L\cos\theta\cos\phi & 0 & 0 & \left(\frac{\rho_c L}{3}+m_k\right)L^2\cos^2\phi & 0 & 0 \\ -\left(\frac{\rho_c L}{2}+m_k\right)L\sin\theta\sin\phi & \left(\frac{\rho_c L}{2}+m_k\right)L\cos\phi & 0 & 0 & \left(\frac{\rho_c L}{3}+m_k\right)L^2 & 0 \\ (m_k+\rho_c L)\sin\theta\cos\phi & (\rho_c L+m_k)L\sin\phi & 0 & 0 & 0 & 1 \end{bmatrix} \tag{10}$$

and

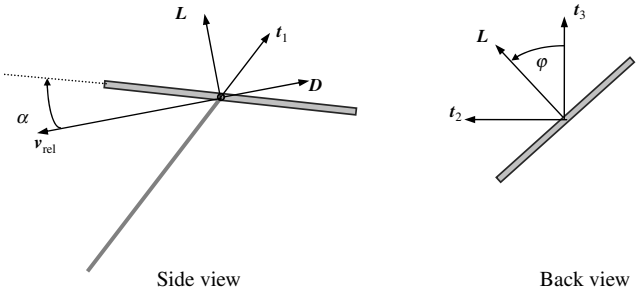

Fig. 2 Lift and drag forces on the kite.

$$\bar{F}_R = \mu_0 + \mu_1 \frac{\sqrt{\dot{x}^2 + \dot{y}^2}}{30} + \mu_2 \frac{(\dot{x}^2 + \dot{y}^2)^2}{30^4} \tag{17}$$

The generalized forces appearing on the right-hand side of Eqs. (11–16) are derived in the following subsections. It is important to point out that the vehicle's speed and direction is controlled only by movement of the kite. There is no active steering assumed on the vehicle itself. Hence, the wheels are assumed to be fully pivotable to enable no-slip rolling of the vehicle in any direction. This means that the vehicle will generally accelerate in the direction of the tether unless it is prevented from doing so (by physical constraints or by drag and rolling resistance). Future work should consider simultaneous control of the kite and onboard steering control.

1. Generalized Forces

The major external forces acting on the kite-tow system that are not modeled thus far in the equations of motion are the lift and drag forces from the kite, together with the drag forces on the tether and ground vehicle. The kite is assumed to be controlled by manipulating its angle of attack and roll angle. Thus, in this study, its attitude dynamics are ignored. In reality, the kite will most likely be controlled using moveable attachment points on the kite wing tips [24].

The lift and drag forces due to the kite are derived using a velocity coordinate system, as shown in Fig. 2. The vector that defines the plane containing the drag force and the velocity vector is given by

$$\boldsymbol{t}_2 = \frac{\boldsymbol{t}_1 \times \boldsymbol{v}_{\text{rel}}(s=L)}{|\boldsymbol{t}_1 \times \boldsymbol{v}_{\text{rel}}(s=L)|} \tag{18}$$

where $\boldsymbol{t}_1 = \sin\theta\cos\phi\boldsymbol{i} + \sin\phi\boldsymbol{j} + \cos\theta\cos\phi\boldsymbol{k}$ is a vector tangential to the cable, and

$$\boldsymbol{v}_{\text{rel}}(s) = \dot{\boldsymbol{r}}(s) - (W_x\boldsymbol{i} + W_y\boldsymbol{j} + W_z\boldsymbol{k}) \tag{19}$$

In general, the components of the wind velocity (W_x, W_y, W_z) are functions of altitude. The lift force, when the roll angle is zero, is parallel to the vector

$$\boldsymbol{t}_3 = \frac{\boldsymbol{v}_{\text{rel}}(s=L) \times \boldsymbol{t}_2}{|\boldsymbol{v}_{\text{rel}}(s=L) \times \boldsymbol{t}_2|} \tag{20}$$

Note that the roll angle is not the conventional body roll angle, but is defined in such a way that it represents the tilt of the lift vector relative to the tether direction.

Hence, the lift and drag force vectors are defined according to

$$\begin{aligned} \boldsymbol{L} &= \tfrac{1}{2}\rho C_L S|\boldsymbol{v}_{\text{rel}}(s=L)|^2(\boldsymbol{t}_2\sin\varphi + \boldsymbol{t}_3\cos\varphi), \\ \boldsymbol{D} &= -\tfrac{1}{2}\rho C_D S|\boldsymbol{v}_{\text{rel}}(s=L)|\boldsymbol{v}_{\text{rel}}(s=L) \end{aligned} \tag{21}$$

Thus,

$$F_x^k = (\boldsymbol{D}+\boldsymbol{L})\cdot\boldsymbol{i}, \quad F_y^k = (\boldsymbol{D}+\boldsymbol{L})\cdot\boldsymbol{j}, \quad F_z^k = (\boldsymbol{D}+\boldsymbol{L})\cdot\boldsymbol{k} \tag{22}$$

The generalized torques due to these forces are obtained as

$$Q_\theta^k = F_x^k L\cos\phi\cos\theta - F_z^k L\cos\phi\sin\theta \tag{23}$$

$$Q_\phi^k = -F_x^k L\sin\phi\sin\theta + F_y^k L\cos\phi - F_z^k L\sin\phi\cos\theta \tag{24}$$

$$Q_L^k = F_x^k\cos\phi\sin\theta + F_y^k\sin\phi + F_z^k\cos\phi\cos\theta \tag{25}$$

The drag forces on the tether are derived by assuming that the drag tangential to the tether is negligible. The computation of the drag forces is complicated by the fact that each part of the tether is moving at a different speed. Therefore, the tether is discretized into a series of n_e elements so that the contributions of drag from each element can be summed to obtain the total drag force and torque due to the tether. The magnitude of the relative wind component tangential to the cable is given by

$$\begin{aligned} \boldsymbol{v}_{\text{rel}}(s)\cdot\boldsymbol{t}_1 &= \dot{L} + (\dot{x} - W_x)\cos\phi\sin\theta + (\dot{y} - W_y)\sin\phi \\ &\quad + (\dot{z} - W_z)\cos\phi\cos\theta \end{aligned} \tag{26}$$

The components of velocity normal to the cable are computed from

$$\boldsymbol{v}_n = \boldsymbol{v}_{\text{rel}}(s) - [\boldsymbol{v}_{\text{rel}}(s)\cdot\boldsymbol{t}_1]\boldsymbol{t}_1 \tag{27}$$

The contribution of the tether drag due to the generalized forces are obtained as

$$\begin{aligned} F_x^t &= -\sum_{j=1}^{n_e}\frac{1}{2}\rho_j C_n d\frac{L}{n_e}\boldsymbol{v}_{n_j}|\boldsymbol{v}_{n_j}|\cdot\frac{\partial\boldsymbol{r}_j}{\partial x} \\ &= -\sum_{j=1}^{n_e}\frac{1}{2}\rho_j C_n d\frac{L}{n_e}|\boldsymbol{v}_{n_j}|\{\dot{x} - W_x - s_j\dot{\phi}\sin\phi\sin\theta \\ &\quad + s_j\dot{\theta}\cos\phi\cos\theta + (W_x - \dot{x})\cos^2\phi - (W_x - \dot{x})\cos^2\phi\cos^2\theta \\ &\quad + (W_y - \dot{y})\cos\phi\sin\theta\sin\phi + (W_z - \dot{z})\cos^2\phi\sin\theta\cos\theta\} \end{aligned} \tag{28}$$

$$\begin{aligned} F_y^t &= -\sum_{j=1}^{n_e}\frac{1}{2}\rho_j C_n d\frac{L}{n_e}\boldsymbol{v}_{n_j}|\boldsymbol{v}_{n_j}|\cdot\frac{\partial\boldsymbol{r}_j}{\partial y} \\ &= -\sum_{j=1}^{n_e}\frac{1}{2}\rho_j C_n d\frac{L}{n_e}|\boldsymbol{v}_{n_j}|\{\cos\phi[s_j\dot{\phi} + (W_x - \dot{x})\sin\phi\sin\theta \\ &\quad - (W_y - \dot{y})\cos\phi + (W_z - \dot{z})\sin\phi\cos\theta]\} \end{aligned} \tag{29}$$

$$\begin{aligned} F_z^t &= -\sum_{j=1}^{n_e}\frac{1}{2}\rho_j C_n d\frac{L}{n_e}\boldsymbol{v}_{n_j}|\boldsymbol{v}_{n_j}|\cdot\frac{\partial\boldsymbol{r}_j}{\partial z} \\ &= -\sum_{j=1}^{n_e}\frac{1}{2}\rho_j C_n d\frac{L}{n_e}|\boldsymbol{v}_{n_j}|\{\dot{z} - W_z - s_j\dot{\phi}\sin\phi\cos\theta \\ &\quad - s_j\dot{\theta}\cos\phi\sin\theta + (W_x - \dot{x})\cos^2\phi\cos\theta\sin\theta \\ &\quad + (W_y - \dot{y})\cos\phi\cos\theta\sin\phi + (W_z - \dot{z})\cos^2\phi\cos^2\theta\} \end{aligned} \tag{30}$$

$$\begin{aligned} Q_\theta^t &= -\sum_{j=1}^{n_e}\frac{1}{2}\rho_j C_n d\frac{L}{n_e}\boldsymbol{v}_{n_j}|\boldsymbol{v}_{n_j}|\cdot\frac{\partial\boldsymbol{r}_j}{\partial\theta} \\ &= -\sum_{j=1}^{n_e}\frac{1}{2}\rho_j C_n d\frac{L}{n_e}|\boldsymbol{v}_{n_j}|\{s_j\cos\phi[-(W_x - \dot{x})\cos\theta \\ &\quad + (W_z - \dot{z})\sin\theta + s_j\dot{\theta}\cos\phi]\} \end{aligned} \tag{31}$$

$$\begin{aligned} Q_\phi^t &= -\sum_{j=1}^{n_e}\frac{1}{2}\rho_j C_n d\frac{L}{n_e}\boldsymbol{v}_{n_j}|\boldsymbol{v}_{n_j}|\cdot\frac{\partial\boldsymbol{r}_j}{\partial\phi} \\ &= -\sum_{j=1}^{n_e}\frac{1}{2}\rho_j C_n d\frac{L}{n_e}|\boldsymbol{v}_{n_j}|\{s_j[s_j\dot{\phi} + (W_x - \dot{x})\sin\phi\sin\theta \\ &\quad - (W_y - \dot{y})\cos\phi + (W_z - \dot{z})\sin\phi\cos\theta]\} \end{aligned} \tag{32}$$

The forces on the ground vehicle are assumed to be due to drag, which is modeled using the equations

$$F_x^0 = -\tfrac{1}{2}\rho_0 C_D A_0 \dot{\boldsymbol{r}}_0 |\dot{\boldsymbol{r}}_0| \cdot \boldsymbol{i}, \qquad F_y^0 = -\tfrac{1}{2}\rho_0 C_D A_0 \dot{\boldsymbol{r}}_0 |\dot{\boldsymbol{r}}_0| \cdot \boldsymbol{j}$$
$$F_z^0 = -\tfrac{1}{2}\rho_0 C_D A_0 \dot{\boldsymbol{r}}_0 |\dot{\boldsymbol{r}}_0| \cdot \boldsymbol{k} \tag{33}$$

The complete set of equations of motion may be integrated after first solving the coupled differential equations for the second derivatives of the generalized coordinates together with the normal reaction and tether tension. The resulting equations are cast in state-space form.

2. *Model with Vehicle Heading Constrained*

The equations of motion can be derived for the case in which the heading of the vehicle is constrained. This could be the case in which the vehicle is attached to a rail or when no-slip conditions prevail. Hence, let

$$x = d\cos\psi, \qquad y = d\sin\psi \tag{34}$$

where d is the distance of the vehicle along the rail. Assuming that the heading of the vehicle is constant, $\dot{\psi} = 0$, then the equations of motion can be written using d as a generalized coordinate instead of x and y. In the interest of brevity, the equations of motion for this case are omitted.

B. Power-Generation Case

In the case in which the ground vehicle is reduced to a stationary ground station containing a winch, the preceding equations can be simplified considerably. The equations of motion are inertially decoupled and can be written in the form

$$\begin{aligned}&(m_k + \tfrac{1}{3}\rho_c L)L^2\ddot{\theta}\cos^2\phi + 2(m_k + \tfrac{1}{2}\rho_c L)L\dot{L}\,\dot{\theta}\cos^2\phi \\ &\quad - 2(m_k + \tfrac{1}{3}\rho_c L)L^2\dot{\theta}\,\dot{\phi}\sin\phi\cos\phi - (m_k + \tfrac{1}{2}\rho_c L)gL\cos\phi\sin\theta \\ &\quad = Q_\theta^k + Q_\theta^t\end{aligned} \tag{35}$$

$$\begin{aligned}&(m_k + \tfrac{1}{3}\rho_c L)L^2\ddot{\phi} + 2(m_k + \tfrac{1}{2}\rho_c L)L\dot{L}\,\dot{\phi} \\ &\quad + (m_k + \tfrac{1}{3}\rho_c L)L^2\dot{\theta}^2\sin\phi\cos\phi - (m_k + \tfrac{1}{2}\rho_c L)gL\sin\phi\cos\theta \\ &\quad = Q_\phi^k + Q_\phi^t\end{aligned} \tag{36}$$

$$\begin{aligned}&(m_k + \rho_c L)\ddot{L} + \tfrac{1}{2}\rho_c\dot{L}^2 - (m_k + \tfrac{1}{2}\rho_c L)L\dot{\phi}^2 \\ &\quad - (m_k + \tfrac{1}{2}\rho_c L)L\dot{\theta}^2\cos^2\phi + (m_k + \rho_c L)g\cos\phi\cos\theta \\ &\quad = Q_L^k - T\end{aligned} \tag{37}$$

The generalized forces are given by Eqs. (23), (24), (31), and (32) and with the components of the velocity of the ground vehicle set to zero.

C. Comparison of a Simple Tether Model with a Multibody Tether Model

The intent of the tether model developed in the previous section is to enable the efficient computation of optimal trajectories while maintaining the basic physics of the system. To ensure that the model reproduces the behavior of more complex models, comparisons were made of the predictions from the simple model with two different multibody models.

To obtain higher-fidelity predictions of the tether motion, it can be modeled using a lumped-parameter approach. In the lumped-parameter (or lumped-mass) approach, the continuous tether is decomposed into a series of point masses connected via elastic or inelastic links. All forces on the tether are applied to the individual masses as a function of their positions and velocities. The lumped-mass approach for modeling cables has been validated on numerous occasions in underwater [25] and aerial environments [26]. The validity of the model depends to a significant degree on the accuracy of the force models. In underwater environments in which the cable often operates at low tensions, bending stiffness and torsion can be important to model accurately. However, for aerial environments, aerodynamic drag and gravity are the dominant external forces.

The aim of comparing the simple model against a more complex model is to validate the overall proposed modeling approach, as well as the equations of motion. First, the case in which the base vehicle remains stationary is considered, followed by a comparison of results generated for a tether pulling a moving vehicle.

1. *Inelastic Flexible Tether Model*

Modeling of flexible cables as completely inelastic introduces additional complexities due to the fact that the cable tension acts as a nonworking constraint force. The equations of motion for such a system can be derived using Lagrange's equations or Kane's equations, which automatically eliminate the nonworking constraint forces from the analysis. Alternatively, the equations can be derived directly via Newton's second law and a set of stabilized constraint equations could be used. The model employed in this paper is derived in [27], in which the tether segments are described using relative spherical coordinates, and the constraint equations are solved in a preelimination step that determines the cable tension to maintain the segments at their specified length. The aerodynamic drag forces are calculated based on the relative velocity of the center of each cable segment using the force defined in Eqs. (31) and (32), based on the local normal relative velocity. The forces on each segment are then lumped to the discrete masses by taking half the force from the adjacent segments.

2. *Elastic Flexible Tether Model*

Treating the tether as inelastic makes it more difficult to handle cases in which one or both end bodies are constrained by forces that are a function of the tether tension, such as the moving vehicle in the kite model. In such cases, it is simpler to determine the tension forces based on a constitutive law such as Hooke's law. Unfortunately, when the tether material has high stiffness, numerical integration can become very inefficient due to the large differences in frequency between the longitudinal modes and the tether string/pendulum modes. This can make elastic models problematic for control law design and trajectory optimization. An elastic tether model is used in this paper to simulate the motion of a tether attached to a moving ground vehicle.

3. *Nonmoving Vehicle Simulation*

A simple case is used to validate the simple tether model. The kite is not included in the simulation. A 40-kg end body, modeled as a sphere, is attached to the end of the tether. The sphere produces a constant vertical lifting force of 944 N and has a projected drag area of $C_D A = 3\ \mathrm{m}^2$. The tether is 500 m long and has a 5-mm diameter, with a line density of 19.63 kg/km. The cable normal drag coefficient is 1.2. The downwind is constant at $W_x = 10$ m/s, whereas a time-varying crosswind component of $W_y = 5\sin(t/30)$ m/s is applied. The air density is assumed to be $1.225\ \mathrm{kg/m}^3$.

Figure 3 shows the results of a simulation with the tether initially pointed vertically upward. Although this starting condition is not realistic, it was chosen because it represents a condition far from equilibrium and is therefore useful for comparing the transient response of the system. The inelastic lumped-mass tether model was run with 40 elements, and the simple tether model was run with various numbers of elements that are used to calculate the tether drag. Results for two extreme cases of 2 elements and 2000 elements are shown. The results illustrate excellent correspondence between all tether models, particularly the crosswind angles. The downwind angle shows a steady-state offset between the flexible and straight tether models caused by the curvature of the tether. Additional simulations with high-drag end bodies that keep the flexible tether relatively straight support this conclusion, in which nearly exact agreement is obtained.

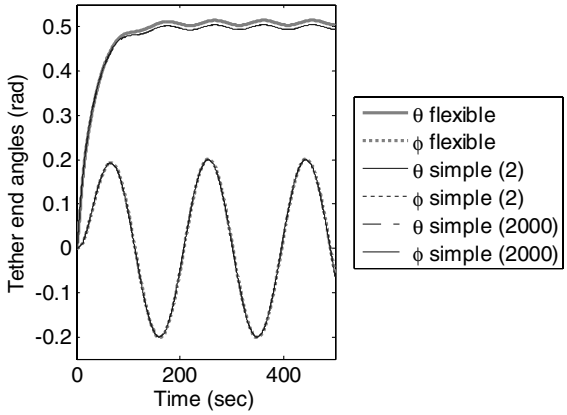

Fig. 3 Comparison of the tether response modeled by a straight rod with distributed drag (number of elements in parentheses) with a 40-element lumped-mass model.

4. Numerical Simulation of a Moving Vehicle

The flexible lumped-mass cable model was simulated with a total tether length of 1000 m, diameter of 2 mm, Young's modulus of 70 GPa, and line density of 3.141 kg/km. The vehicle mass is assumed to be 2000 kg, and the wind speed is constant at $W_x = 5$ m/s. Specified forces are applied to the end of the cable of $F_x = 3000 - 500\cos(t/20)$ N, $F_y = 500\sin(t/30)$ N, $F_z = 10,000$ N, with a tip mass of 50 kg. The C_DA of the vehicle is 1.0 m^2, and the air density is 1.225 kg/m^3. The lumped-mass model is discretized into 15 elements with the cable initially in vertical equilibrium under the action of gravity and the force F_z applied to the end. The vehicle and tether are initially moving in the direction of the wind at 20 m/s. Again, these initial conditions are far from equilibrium. When the simulation begins, there is an initial transient due to the sudden application of drag to the cable. This enables a comparison of the transient effects of cable vibrations on the results. For comparison purposes, the simple model is run with the tether divided into 20 elements for the drag calculations. The difference between 20 and 200 elements is almost negligible.

Numerical results are shown in Fig. 4a for the tether angles and in Fig. 4b for the vehicle velocity. The tether-angle responses show excellent agreement, and both models capture the initial transient effects well. There are small differences in the downwind angle θ, in which the simple model tends to exhibit slightly lower damping than the flexible model. This is because in the flexible model, there is a delay between the bowing of the tether due to drag and its effect on the end of the cable. In the simple model, there is no delay, and all aerodynamic forces correspond to a torque that directly affects the position of the end body. The crosswind angle and steady-state behavior of the downwind angle are in very good agreement. The components of the vehicle velocity are also in good agreement with the results of the flexible tether model. The vehicle initially slows down due to the opposing effects of vehicle drag and friction, before being overcome by the downwind component of tether tension. There is a small difference in the steady-state velocity due to cable curvature and cable elasticity. However, for design purposes, these differences are quite small. Hence, it was demonstrated that the simple tether model is able to produce realistic system responses when compared with higher-fidelity models.

IV. Periodic Optimal Crosswind Trajectories

A. Crosswind Towing

The major objective of this paper is to establish the optimal means of flying the kite to produce the maximum crosswind control action on the ground vehicle, as well as maximum power generation. It is a relatively simple matter to use the system to travel downwind, which would require the system to operate at more or less a constant angle. This is by no means guaranteed to give an optimal solution. Efficient motion in the crosswind direction will require more complex trajectories of the kite. In this section, the best way of flying the kite to maximize the crosswind distance traveled by the vehicle is considered. To guarantee the repeatability of the maneuver for long periods of time, it is useful to derive the trajectory to be periodic. This means that the relative position and velocity of the kite to the vehicle is repeated with some prescribed period. In addition, the planar components of the vehicle velocity also need to be periodic. The inertial position of the vehicle is clearly not periodic under these assumptions. Although it is possible to vary the tether length during towing, this option is not explored in this work. Reference [28] presents some preliminary results detailing this option. Throughout the remainder of this paper, the vehicle motion is assumed to remain planar so that $z = 0$. However, the model and general optimization approach also apply to the case in which the ground is inclined.

The periodic optimal control problem can be stated as follows: Find the (pseudo) control inputs $\boldsymbol{u}(\cdot) = \{\dot{\alpha}, \dot{\varphi}\}$, the maneuver time $t_f - t_0$, and corresponding state trajectory $\boldsymbol{x}(\cdot) = \{x, y, \theta, \phi, \alpha, \varphi, \dot{x}, \dot{y}, \dot{\theta}, \dot{\phi}\}$ that minimizes the cost function

$$J_1 = -\frac{y(t_f)}{t_f - t_0} + W_1(t_f - t_0)\int_{t_0}^{t_f}(\dot{\alpha}^2 + \dot{\varphi}^2)\mathrm{d}t \tag{38}$$

where W_1 is a weighting coefficient that effectively trades the kite control variations with crosswind performance. In this formulation, the period of the maneuver $t_f - t_0$ is free to be optimized. Hence, the cost function is selected to maximize the average crosswind distance traveled per second (average velocity), while minimizing the total control effort. In the case in which the vehicle heading is fixed, the cost function replaces $y(t_f)$ with $d(t_f)$, which maximizes the average vehicle velocity in the prescribed direction.

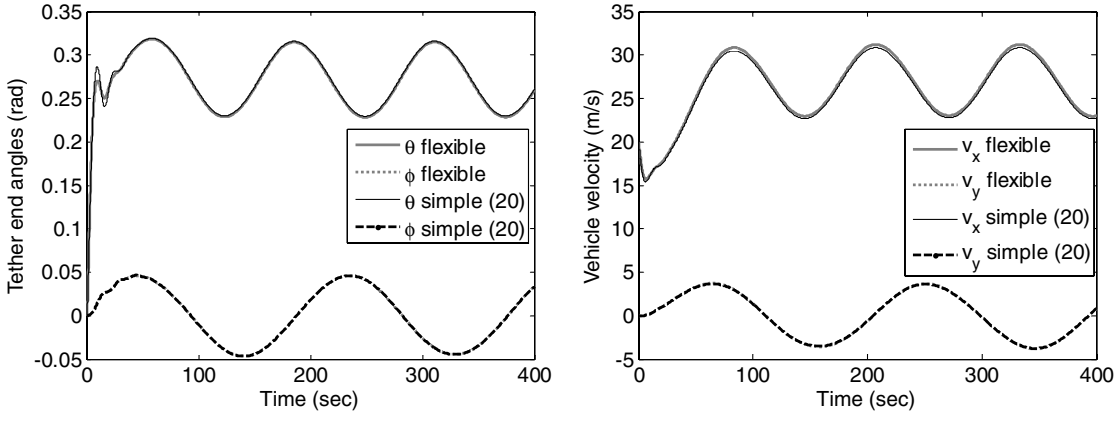

a) b)

Fig. 4 Comparison of the system response with a moving vehicle showing a) angles of the tether tip relative to the vehicle and b) components of vehicle velocity.

The periodicity conditions are given by

$$\{\theta, \phi, \alpha, \varphi, \dot{x}, \dot{y}, \dot{\theta}, \dot{\phi}\}_{t=t_0} = \{\theta, \phi, \alpha, \varphi, \dot{x}, \dot{y}, \dot{\theta}, \dot{\phi}\}_{t=t_f} \tag{39}$$

In addition to the preceding constraints, a path constraint is enforced to ensure that the model remains realistic (rolling resistance is always assumed):

$$\dot{x}^2 + \dot{y}^2 \geq 1 \tag{40}$$

The kite control parameters are constrained by the following constraints:

$$|\alpha| \leq 10 \text{ deg}, \quad |\varphi| \leq 30 \text{ deg}, \quad |\dot{\alpha}| \leq 5 \text{ deg/s}, \quad |\dot{\varphi}| \leq 5 \text{ deg/s} \tag{41}$$

Because the tether cannot sustain compressive forces, a path constraint of the form

$$T \geq T_{\min} \tag{42}$$

must be enforced. In this paper, $T_{\min}$ is set as 10 N. Furthermore, to prevent the kite from impacting the ground, the following constraints are also enforced:

$$|\theta| \leq 80 \text{ deg}, \qquad |\phi| \leq 70 \text{ deg} \tag{43}$$

B. Maximum Power Generation

For maximum power generation, the objective is to maximize the power generated by the system per cycle. The instantaneous power is given by $T\dot{L}$. During one cycle, it is necessary to reel the tether out, then back in again. This means that the tether tension must be judiciously controlled in such a way that the net energy per cycle is positive. In addition, because the kite model is highly simplified, it is desirable to maintain the kite control angles and reel acceleration as smoothly as possible. The control problem is defined as follows: Find the (pseudo) control inputs $\boldsymbol{u}(\cdot) = \{\dot{\alpha}, \dot{\varphi}, \ddot{L}\}$, maneuver time $t_f - t_0$, and corresponding state trajectory

$$\boldsymbol{x}(\cdot) = \{x, y, \theta, \phi, \alpha, \varphi, \dot{x}, \dot{y}, \dot{\theta}, \dot{\phi}, L, \dot{L}\}$$

that minimize the following combined cost function:

$$J_3 = \int_{t_0}^{t_f} \left[-\frac{T\dot{L}}{t_f - t_0} + (W_2\dot{\alpha}^2 + W_3\dot{\varphi}^2 + W_4\ddot{L}^2) \right] \mathrm{d}t \tag{44}$$

where W_2, W_3, and W_4 are constant weighting coefficients. Here, the cycle period can be optimized to give the maximum average power per cycle. The system is subject to a minimum tension constraint given by Eq. (42) and the periodicity constraints

$$\{\theta, \phi, \alpha, \varphi, \dot{x}, \dot{y}, \dot{\theta}, \dot{\phi}, L, \dot{L}\}_{t=t_0} = \{\theta, \phi, \alpha, \varphi, \dot{x}, \dot{y}, \dot{\theta}, \dot{\phi}, L, \dot{L}\}_{t=t_f} \tag{45}$$

The tether angles are constrained according to Eq. (43). The following additional constraints are imposed on the reeling:

$$\left| \frac{\Delta L}{L_{\text{ref}}} \right| \leq 0.3, \qquad |\dot{L}| \leq 10 \text{ m/s}, \qquad |\ddot{L}| \leq 3 \text{ m/s}^2 \tag{46}$$

Note that control of the tether length is assumed to be achieved by manipulation of $\ddot{L}$ (i.e., the reel acceleration). This is preferable to using the length rate directly because it ensures that the reel rate remains continuous.

C. Numerical Method

The optimal control problems defined in the preceding subsections are solved using the Legendre pseudospectral method. The Legendre pseudospectral method has found wide appeal for solving optimal control problems due to its accuracy and simplicity [29,30]. Essentially, this approach discretizes the states and controls using Lagrange interpolating polynomials expanded at the Legendre–Gauss–Lobatto (LGL) points for a specified order-N polynomial. The consequence of this choice is that the optimization parameters are the values of the states and controls themselves, as opposed to polynomial coefficients that usually do not have a physical meaning. In addition, the cost function is easily discretized by means of a Gauss–Lobatto quadrature. The state equations are enforced in an approximate fashion by differentiating the interpolating polynomials for the states and employing an equality constraint at each LGL point. The equality constraints require the state derivatives to be equal to the vector field at the corresponding LGL point. Studies of convergence behavior and application of the method can be found in [30]. The accuracy of the solution for a particular problem is, in general, dependent on the degree of discretization N. Although pseudospectral methods produce exponentially accurate solutions for smooth problems, implying small values for N, a large value of N was used to produce the results in this paper ($N = 160$). In fact, recent results demonstrate that suitably small values of N can be used even for nonsmooth problems if combined with an anti-aliasing strategy [31]. Feasibility of the primal solution can be easily established by propagating the control signals using a standard Runge–Kutta algorithm [32].

When solving the resulting nonlinear programming problem, there is no guarantee that the solution obtained is the global minimum. In this work, different random guesses were used to obtain as many varied local minima as possible. The best resulting trajectory was then used as the nominal baseline.

V. Numerical Results

A. Kite-Pulling Case

1. *Vehicle Heading Fixed*

Optimal trajectories for the system were generated with the tether divided into 10 elements for computation of the drag forces. The assumed system parameters that are used for this analysis are given in Table 1. It is important to note that the precise values that are used here are not important. The goal of this study is to develop an understanding of the general form of the optimal maneuvers required for crosswind towing and/or power generation. Variations in the parameters are used to establish the sensitivity of the system performance. The mass of the vehicle that is used for towing is made relatively large to ensure that the model remains valid (i.e., the vehicle is always in contact with ground). The weighting coefficient $W_1 = 10^{-3}$ was selected.

Figure 5a shows the variation of the average optimal vehicle velocity when its heading is constrained. A rail angle of $\psi = 0$ implies that the vehicle heads directly downwind. The results show that this is not the optimal angle with which to tow the vehicle. In fact, the optimal angle is almost 90 deg. This is explained by the fact that as the vehicle moves parallel to the wind, the relative air speed at the kite drops, reducing the forces generated by the kite. Hence, at $\psi = 0$, the average vehicle velocity is less than the wind speed of

Table 1 Nominal system parameters

Parameter	Nominal value
Kite mass	50 kg
Vehicle mass	2000 kg
Tether length L	1000 m[a]
Tether density ρ_c	3.141 kg/km
Tether diameter d	2 mm
Cable normal drag coefficient C_{D_N}	1.2
Vehicle projected drag area $C_D A$	1.0
Friction coefficients $[\mu_0, \mu_1, \mu_2]$	[0.1, 0.01, 0.001]
Lift curve slope C_{L_α}	4.4/rad
Zero-lift drag C_{D_0}	0.02
Lift-induced drag K	0.1
Kite wing area S	25 m^2
Scale height h_s	100 m
Wind power-law index	0.1

[a]The nominal length for power generation is 2000 m.

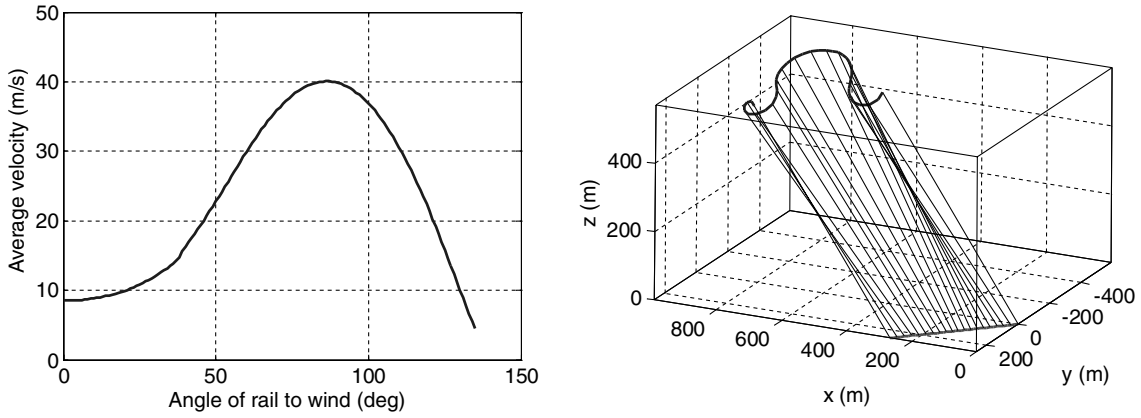

a) b)

Fig. 5 Optimal results for towing with heading constrained: a) effect of rail angle on the optimal average vehicle velocity and b) optimal trajectory in the inertial frame for $\psi = 45$ deg (right).

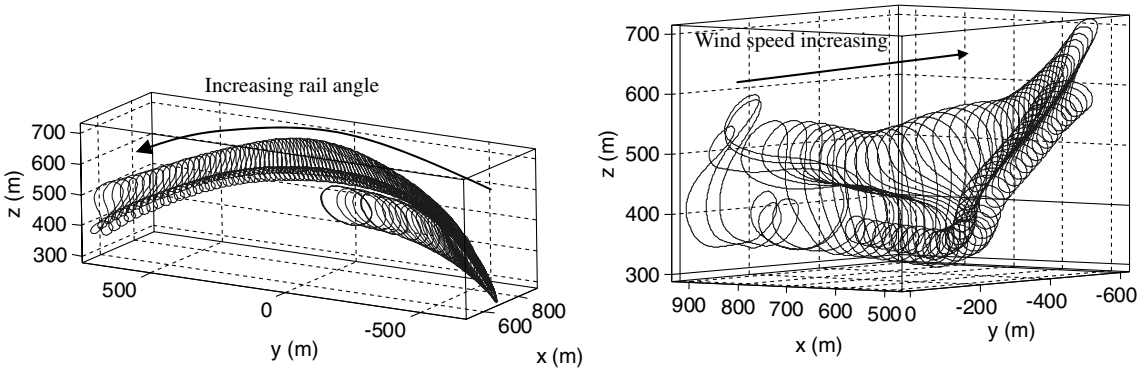

a) b)

Fig. 6 Optimal kite trajectories for a ground vehicle towed on a rail shown relative to the vehicle as a) a function of the rail angle and b) a function of wind speed for $\psi = 45$ deg.

10 m/s. As the rail angle increases, the kite sees a larger component of relative velocity due to its higher speed normal to the wind direction. The tension forces from the tether are required to overcome the drag and rolling resistance of the vehicle only. Beyond $\psi = 90$ deg, the vehicle is heading into the wind, and the kite effectiveness decreases. Figure 5b shows an example of the system trajectory for the specific case in which $\psi = 45$ deg.

Figure 6a shows the optimal kite trajectories that maximize the vehicle's average velocity with the heading constrained. The results illustrate that for downwind travel, the optimal solution is not to keep the kite stationary relative to the vehicle, but rather to fly it in a circle. This increases the relative airspeed and hence the lift forces that can be used for towing. Increasing the rail angle initially causes the kite to fly circles/ellipses that are progressively offset from the vehicle path until $\psi \approx 38$ deg, when the patterns become more complex than circles/ellipses. The kite trajectories for heading angles between $\psi = 38$ and 135 deg show that the shape of the trajectories does not vary substantially.

Figure 6b shows a family of kite trajectories for wind speeds in the range of 5 to 15 m/s for the case in which $\psi = 45$ deg. The low-wind-speed conditions require the kite to perform large looping maneuvers to maximize its relative airspeed. Increasing the wind speed leads generally to an increase in the mean altitude of the kite. Although not shown here, the optimal trajectories demand the maximum angle of attack from the kite across the entire trajectory. Flying the kite at the maximum angle of attack maximizes the tether tension. Hence, for a given maximum lift coefficient, the kite forces are governed solely by the roll angle and relative airspeed. Therefore, optimal towing conditions can be generated by making the kite fly tighter trajectories at higher wind speeds. However, this result may depend on the assumed lift and drag properties of the kite and is not necessarily optimal for all configurations.

Figure 7 shows the effect of variations in the system parameters on the optimal average vehicle velocity for the case $\psi = 45$ deg. The results show that the cable length must be appropriately chosen because long cables can degrade performance (for a fixed-diameter tether). This is largely the result of increased tether drag and weight with cable length, which prohibits larger motions of the kite. In this particular case, a tether length half of the nominal improves performance by 8%. Changes in the kite area lead to an almost linear change in average vehicle velocity. However, the optimal results indicate that reducing the kite area by 50% leads to an approximate 60% reduction in system effectiveness. Changes to the kite mass produce only moderate changes in the average vehicle velocity. Decreasing the kite mass leads to an increase in performance of only a few percent. In contrast, changes in the vehicle friction (rolling) coefficient leads to large changes in performance. This is due to the fact that rolling friction is a significant dissipation of energy in the system. Doubling the friction coefficient leads to a decrease of approximately 25% in average vehicle velocity. Similar conclusions are apparent by examining the effects of vehicle mass. The resistance forces are proportional to vehicle mass and, hence, one would expect there to be a nearly direct correspondence between changing the friction coefficient and vehicle mass. However, the rolling resistance is also dependent upon the vehicle velocity. The results show that doubling the vehicle mass decreases performance by approximately 40% compared with the nominal case. Finally, the system performance is most strongly influenced by the wind speed. The numerical results show that the variation in average vehicle velocity with wind speed is approximately cubic.

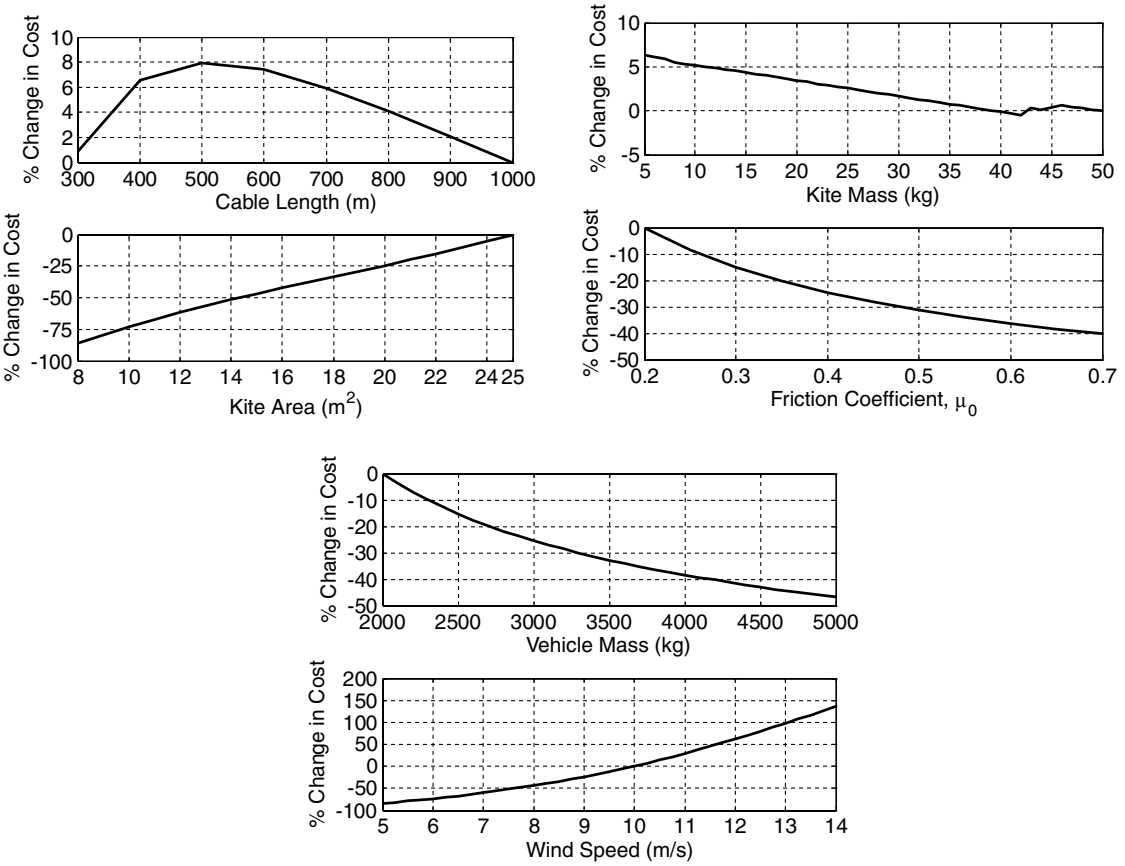

Fig. 7 Effect of changes in the system parameters on the optimal average vehicle velocity for $\psi = 45$ deg.

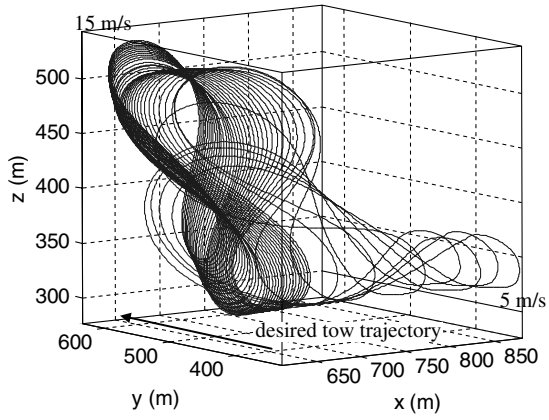

Fig. 8 Optimal kite trajectories for towing a ground vehicle (relative to vehicle), shown as a function of wind speed.

2. Free Vehicle Heading

In this section, results generated for the case in which the vehicle heading is free are calculated. Figure 8 shows the optimal kite trajectories relative to the ground vehicle as a function of wind speed. All trajectories are approximately figure-eight maneuvers. When the wind speed is comparatively low, the kite maximizes its relative airspeed by flying predominantly in a direction transverse to the wind with variations in altitude of approximately 100 m. The trajectories are most sensitive at low wind speed due to the limited lift that can be generated. Small changes in wind speed lead to large changes in the kite forces and therefore dramatic variations in the performance of the system. This can be seen as the kite trajectories shift more toward the desired tow direction. To maximize the tension forces in the crosswind direction, the kite trajectories become vertical figure eights. This is possible at high wind speeds because the lift forces on the kite are significantly larger. The resulting trajectories are also less sensitive to changes in the wind speed at high speeds.

Figure 9 shows the results of a sensitivity analysis of the optimal solutions to variations in the nominal system parameters. The results illustrate that the cable length used in the case in which the heading of the vehicle is unconstrained is nearly optimal for the nominal system. In fact, increasing the cable length to approximately 1200 m leads to an increase in performance of about 1.3%. Substantial increases in length lead to a degradation in performance, as do reductions in the cable length. The effect of kite area on the results is nonlinear so that small changes in kite area around the nominal produces comparatively small changes in performance. On the other, there is a substantial reduction in performance if the kite area is too small. Reducing the kite area by 50% leads to an approximate 37% reduction in performance, whereas the performance reduction is nearly 83% for a 68% reduction in area. The kite mass is the least sensitive parameter in the system, for which an 80% reduction in kite mass leads to only a 3.65% improvement in performance. Changes in the friction coefficient and vehicle mass lead to roughly similar changes in performance, in which, for example, doubling the vehicle mass or friction coefficient decreases performance by about 15%. Finally, the sensitivity to wind speed is the most significant, for which changing the speed by $\pm 50\%$ leads to changes of $\pm 72\%$ in performance. Unlike the previous case, the crosswind performance does not vary cubically with wind speed, but is closer to being a quadratic variation. This is due to the fact that increasing wind speed also increases drag on the system, which tends to pull the system downwind, thereby reducing crosswind performance.

B. Power-Generation Case

The power-generation case is extremely important because it forms the basis of future laddermill technology. The nominal system parameters are the same ones used for the towing case shown previously in Table 1, except that the nominal tether length is 2 km rather than 1 km. The weighting coefficients in the cost function were

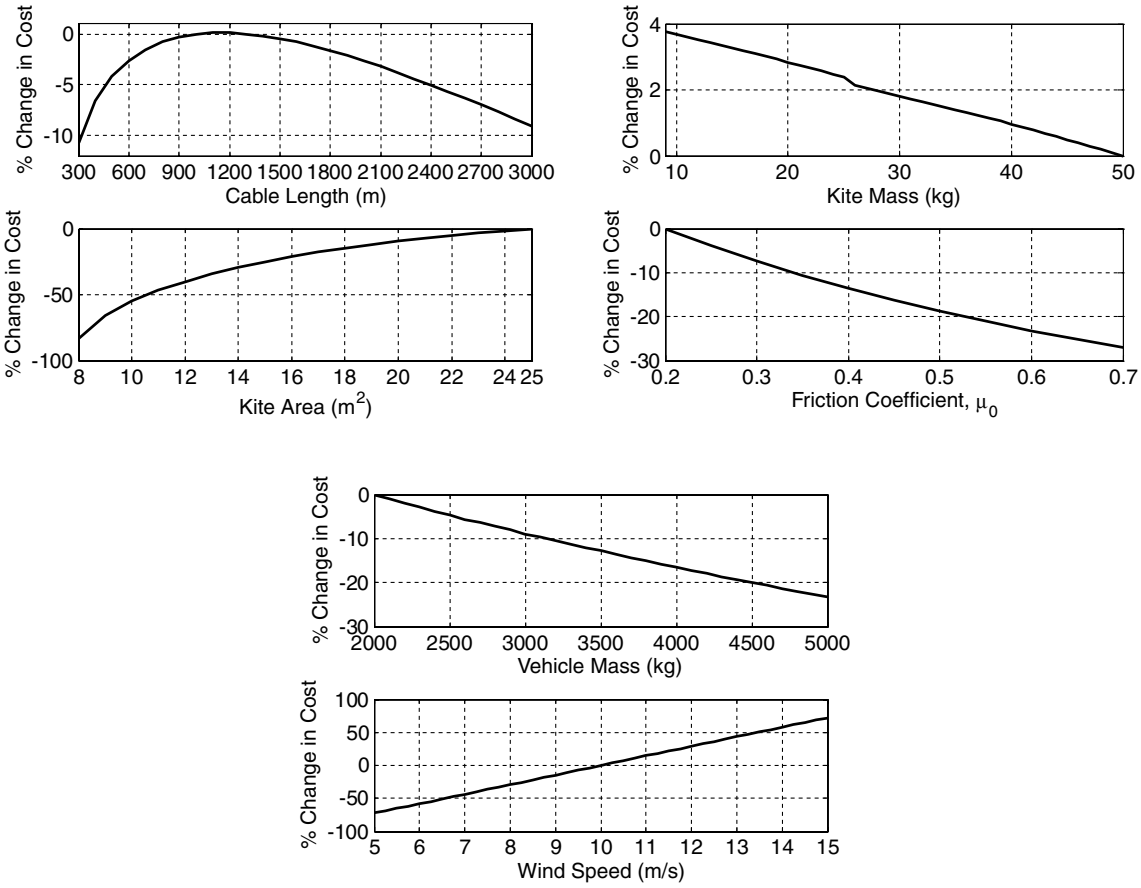

Fig. 9 Effect of changes in system parameters on the optimal crosswind vehicle velocity (heading unconstrained).

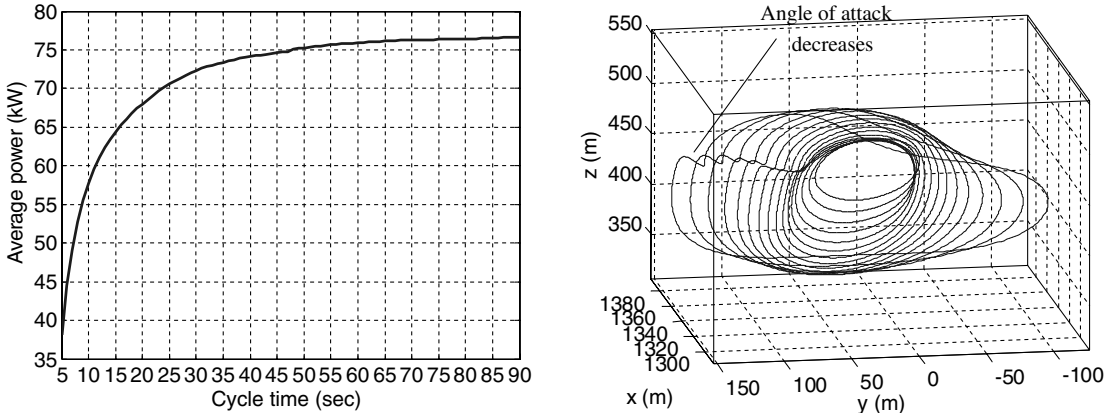

a) **b)**

Fig. 10 Optimal power-generation results: a) average power generated by the kite system as a function of cycle time and b) optimal kite trajectories for cycle times between 5 and 20 s.

selected as $W_2 = W_3 = W_4 = 10^{-2}$. Direct optimization of the system with a free period has been performed [28], but it is of interest to understand the behavior of the power production for different cycle times. Hence, Fig. 10a shows the average power generated by the system as a function of cycle time. This illustrates an approximate logarithmic relationship between average power and cycle time. Increasing the cycle time is beneficial because it leads to improved performance. However, the average power generated appears to asymptote to a value less than about 80 kW for the nominal parameters. Hence, for practical purposes, the cycle time could be fixed at a desired value of about 60 s to provide a good compromise between cycle length and average power per cycle. A reduction of the cycle time from 60 to 25 s leads to a decrease in performance of about 8%, whereas further reductions cause an exponential decrease in effectiveness. Hence, the cycle time is very important for producing an optimal system, and it must be selected large enough (or optimized) to give the best performance. Figure 10b shows the optimal kite trajectories for cycle times between 5 and 20 s (i.e., least efficient). For a cycle time of 5 s, the optimal trajectory is nearly a perfect circle. As the cycle time increases, the kite flies more transversely to the wind direction in elliptical trajectories. The ability to generate significant power is largely determined by the difference in tension between the reel-out and reel-in portions of the trajectory. The point at which the kite angle of attack is decreased is evident in Fig. 10b as a nearly horizontal movement of the kite parallel to the wind direction. This is produced by the rapid reel-in of the tether. The speed at which the tether can be reeled in is determined by the combination of cycle time and reel-rate constraint. Hence, increasing

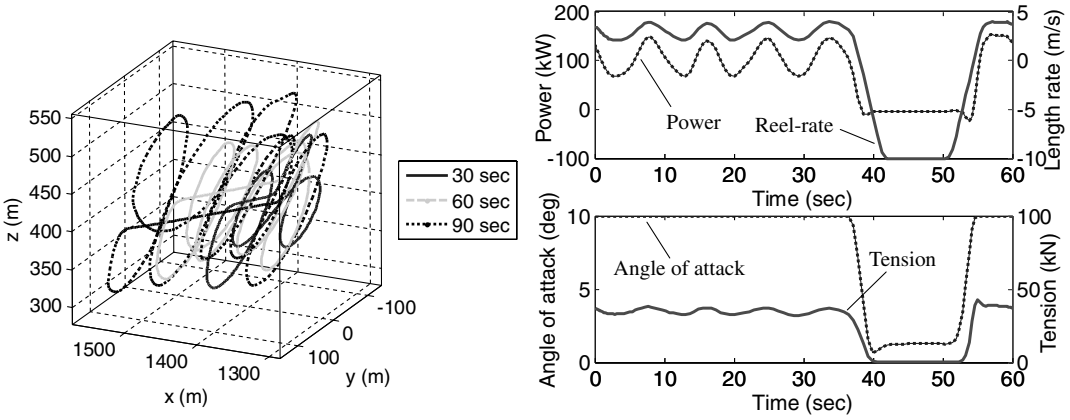

a) b)

Fig. 11 Optimal power-generating kite trajectories: a) examples with 30-, 60-, and 90-s periods and b) example of power generation for a cycle time of 60 s (average power is 75.93 kW).

the cycle time initially allows the tether to be progressively reeled in at higher speeds. However, once the reel rate saturates, only relatively moderate improvements in the performance are possible. The reel rate first saturates for a cycle time of approximately 18 s. This is one of the main reasons for the asymptotic behavior of the power generation versus cycle time. It should also be noted that the constraints on the allowable tether angles and tether length also play a role in the results. In the nominal case, the optimal solution tries to keep the tether length as short as possible and flies the kite to meet the minimum θ requirement (less than 80 deg). Altering the values of the constraints would almost certainly alter the resulting performance. It is also expected that further increases in cycle time would lead to a situation in which the system will perform multiple periods of power generation within one cycle. This is because the cable cannot be reeled out indefinitely, and the definition of the cost function is average power, not total power.

Figure 11a shows examples of the optimal kite trajectories for cycle times of 30, 60, and 90 s. The trajectories are consistent in altitude, as well as in their general characteristics. However, as the cycle time increases, the kite performs larger loops to increase the relative air speed. All of the optimal trajectories consist of a period in which the tether is reeled in at the maximum reel rate, which occurs at a nearly constant altitude. Figure 11b shows examples of the variation in power, reel rate, kite angle of attack, and tension during an optimal power-generation trajectory. The results show that the kite angle of attack is maintained at the maximum value when the tether is reeled out. The maneuvering of the kite due to variations in roll angle induce changes in the cable tension. Peaks in tension also correspond to peaks in the reel rate and hence local peaks in the instantaneous power output. When the tether is reeled in, the kite angle of attack is reduced to a level that maintains the tension at its lower bound. The amount of power required to retrieve the tether is very small (∼4–5 kW on average), despite the fact that the reel-in speed is higher than the reel-out speed. It should be noted that because the kite drag grows with the square of the lift coefficient, higher allowable maximum angles of attack could alter the conclusion that operating at the maximum angle of attack is optimal during the reel-out phase.

Figure 12 summarizes the sensitivity of the optimal power-generation trajectory for a 60-s cycle time. The power-generation trajectories are significantly more sensitive than the crosswind towing trajectories. The optimal average power varies approximately linearly with kite area, except for very small kite areas. For example, an area of 5 m^2 produces an almost infeasible problem (nearly no power can be produced). Increasing the kite drag coefficients C_{D_0} and K by a factor of 2 reduces the optimal power production by approximately 65%. Further increases in the drag coefficients also lead to a situation in which almost no power can be produced. The system is least sensitive to the kite mass, with less than 0.1% change in power output with a reduction in kite mass of 50%. The effect of variations in the wind model shows that the wind speed at the kite's altitude plays a very significant role in the amount of power that can be generated by the system. In particular, for higher power-law indexes (∼0.33), nearly double the power can be generated. The magnitude of the wind is the most significant factor in determining the system power output when a cubic dependency is evident. In particular, increasing the wind speed by 50% to 15 m/s roughly triples the power output of the system. Design of the tether parameters is also extremely important to ensure optimal power production. The results show that the tether diameter should be kept as small as possible to minimize weight and drag. Doubling the tether diameter leads to nearly a 50% reduction in power output. Tether drag is responsible for reducing the kite altitude and therefore the relative wind at the kite. The power output varies approximately linearly with changes in the tether drag coefficient. Therefore, methods for minimizing the cable drag could help to improve the system efficiency. However, the results show that the key parameter for power generation is proper selection of the tether length. The reason for this is the combined reduction in weight and drag. The optimal solution for a 2-km-long tether keeps the kite at relatively low altitudes (∼500 m). Therefore, improved performance is achieved by adjusting the tether length to be appropriate to the optimal altitude. The power output increases almost exponentially as the tether length decreases. A tether length of 300 m increases the power output by over 4000%. This is due to the reduced total cable drag, which leads to higher lift/drag ratios of the complete system, leading to higher achievable kite speeds. On the other hand, increasing the tether length does not seriously reduce the power output below the nominal value. Hence, in a given operating environment, the tether length should be adjusted judiciously to give the maximum power production possible from the system. In reality, the wind can change quite dramatically with time. A shorter cable length would lead to higher sensitivity to winds. Longer tethers result in systems that are generally easier to fly and there is more tolerance for correcting errors in kite altitude than with shorter tethers. In addition, the higher tensions induced in shorter tethers mean that thicker cables would be required, which would ultimately decrease performance. Thus, there is a compromise between efficiency and system reliability when selecting an appropriate tether length.

C. Design Implications for a Practical System

The cable tension shown in Fig. 11b peaks at about 40 kN, which would exceed the tensile strength of a cable 2 mm in diameter using currently available materials. Hence, the nominal system operating at the optimal conditions could not be currently flown by a practical system. This means that the cable diameter would need to be increased to sustain the loads. However, as the results in Fig. 12 illustrate, increasing the cable diameter to a reasonable value of about 8 mm (to sustain 40 kN at a stress of ∼800 MPa) dramatically reduces the system's effectiveness. In reality, however, increasing cable diameter increases weight and drag, which would slow the

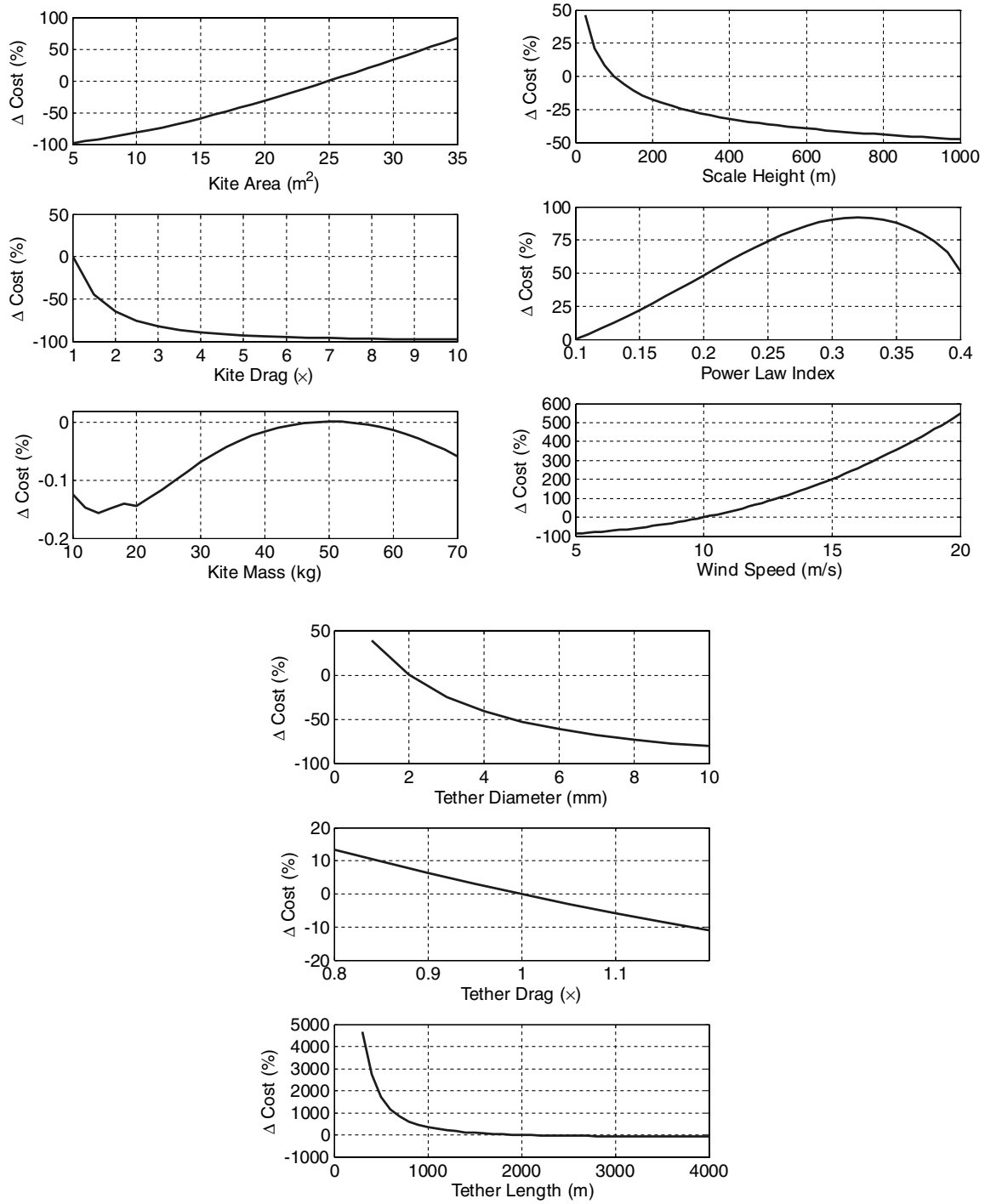

Fig. 12 Effect of changes in the system parameters on the optimal power generation for a 60-s cycle time.

kite's speed and hence reduce tension. Thus, the system trajectory and cable design must be carefully selected to optimize the overall power-generation performance. Alternatively, given the cable material strength and diameter, an additional upper tension constraint can be placed on the trajectory design. As an example, for a cycle time of 60 s, an upper constraint of 25 kN on the tension results in an average power output of 68.7 kW compared with 75.9 kW without the constraint. Hence, the efficiency of the system does not appear to be seriously compromised.

VI. Conclusions

Optimal control of a three-dimensional tethered kite system was considered for optimizing the crosswind dynamics. Two potential applications, towing of a ground vehicle and power generation, were studied by using numerical optimal control. A simplified dynamic model of the system was derived to enable efficient, but representative, solutions. In the case of crosswind towing, results show that higher wind speeds are able to produce more useful work for towing the vehicle across the wind. In the case of optimal power generation, complex trajectories were generated as a function of cycle time. The results show that the kite makes very efficient use of crosswind motions to generate significantly higher aerodynamic forces, which results in larger tensions. The results also demonstrate that the average power generated by the system increases with the cube of the wind velocity. Proper design of the system is required to maximize the average power output from the system per cycle.

References

[1] Carpenter, H. G., "Tethered Aircraft Having Remotely Controlled Angle of Attack," U.S. Patent 5,931,416, issued 3 Aug. 1999.

[2] Carpenter, H. G., "Tethered Aircraft System for Gathering Energy From Wind," U.S. Patent 6,254,034, issued 3 July 2001.
[3] Emeis, S., and Türk, M., "Comparison of Logarithmic Wind Profiles and Power Law Wind Profiles and their Applicability for Offshore Wind Profiles," *Wind Energy: Proceedings of the Euromech Colloquium*, edited by Peinke, J., Schaumann, P., Barth, S., Springer, Berlin, 2007, pp. 61–64.
[4] Emeis, S., "How Well Does a Power Law Fit to a Diabetic Boundary-Layer Wind Profile?," *DEWI Magazine*, No. 26, Feb. 2005, pp. 59–62.
[5] Sagrillo, M., "Site Analysis for Wind Generators, Part 1: Average Wind Speed," *Home Power*, Vol. 40, Apr.–May 1994, pp. 86–90.
[6] Hussain, M., "Dependence of Power Law Index on Surface Wind Speed," *Energy Conversion and Management*, Vol. 43, No. 4, 2002, pp. 467–472.
doi:10.1016/S0196-8904(01)00032-2
[7] Fletcher, C. A. J., and Roberts, B. W., "Electricity Generation from Jet-Stream Winds," *Journal of Energy*, Vol. 3, July–Aug. 1979, pp. 241–249.
[8] Manalis, M. S., "Airborne Windmills: Energy Source for Communication Aerostats," AIAA Lighter Than Air Technology Conference, AIAA Paper 75-923, July 1975.
[9] Manalis, M. S., "Airborne Windmills and Communication Aerostats," *Journal of Aircraft*, Vol. 13, No. 7, 1976, pp. 543–544.
[10] Riegler, G., and Riedler, W., "Tethered Wind Systems for the Generation of Electricity," *Journal of Solar Energy Engineering*, Vol. 106, May 1984, pp. 177–181.
[11] Riegler, G., Riedler, W., and Horvath, E., "Transformation of Wind Energy by a High-Altitude Power Plant," *Journal of Energy*, Vol. 7, No. 1, 1983, pp. 92–94.
[12] Roberts, B. W., and Shepards, D. H., "Unmanned Rotorcraft to Generate Electricity Using Upper Atmospheric Winds," *Proceedings of the Tenth Australian International Aerospace Congress* [CD-ROM], edited by D. J. Mee, Engineers Australia, Brisbane, Australia, July 2003, Paper AIAC 2003-098.
[13] Fletcher, C. A. J., "On the Rotary Wing Concept for Jet Stream Electricity Generation," *Journal of Energy*, Vol. 7, No. 1, 1983, pp. 90–92.
[14] Rye, D. C., "Longitudinal Stability of a Hovering, Tethered Rotorcraft," *Journal of Guidance, Control, and Dynamics*, Vol. 8, No. 6, 1985, pp. 743–752.
[15] Biscomb, L. I., "Multiple Wind Turbine Tethered Airfoil Wind Energy Conversion System," U.S. Patent 4,285,481, issued 25 Aug. 1981.
[16] Watson, W. K., "Airship-Floated Wind Turbine," U.S. Patent 4,491,739, issued 1 Jan. 1985.
[17] Ockels, W. J., "Laddermill, a Novel Concept to Exploit the Energy in the Airspace," *Aircraft Design*, Vol. 4, No. 2, 2001, pp. 81–97.
doi:10.1016/S1369-8869(01)00002-7
[18] Meijaard, J. P., Ockels, W. J., and Schwab, A. L., "Modelling of the Dynamic Behaviour of a Laddermill, A Novel Concept to Exploit Wind Energy," *Proceedings of the Third International Symposium on Cable Dynamics*, Association of Engineers from the Montefiore Electrical Inst., Liege, Belgium, Aug. 1999, pp. 229–234.
[19] Lansdorp, B., and Ockels, W. J., "Comparison of Concepts for High-Altitude Wind Energy Generation with Ground Based Generator," *Proceedings of the Second China International Renewable Energy Equipment and Technology Exhibition and Conference (NRE2005)*, Ministry of Natural Resources and Environment, Beijing, pp. 409–417.
[20] Lansdorp, B., Remes, B., and Ockels, W. J., "Design and Testing of a Remotely Controlled Surfkite for the Laddermill," World Wind Energy Conference, Melbourne, Australia, Nov. 2005.
[21] Lansdorp, B., and Williams, P., "The Laddermill: Innovative Wind Energy from High Altitudes in Holland and Australia," *Proceedings of the Global Windpower 2006 Conference* [CD-ROM], Australian Wind Energy Association, Melbourne, Australia, Sept. 2006.
[22] Loyd, M. L., "Crosswind Kite Power," *Journal of Energy*, Vol. 4, No. 3, 1980, pp. 106–111.
[23] Kiencke, U., and Nielsen, L., *Automotive Control Systems: For Engine, Driveline, and Vehicle*, 2nd ed., Springer–Verlag, Berlin, 2005, p. 332.
[24] Williams, P., Lansdorp, B., and Ockels, W., "Flexible Tethered Kite with Moveable Attachment Points, Part 1: Dynamics and Control," AIAA Paper 2007-6628, Aug. 2007.
[25] Driscoll, F. R., Lueck, R. G., and Nahon, M., "Development and Validation of a Lumped Mass Dynamics Model of a Deep-Sea ROV System," *Applied Ocean Research*, Vol. 22, No. 3, 2000, pp. 169–182.
doi:10.1016/S0141-1187(00)00002-X
[26] Williams, P., Lapthorne, P., and Trivailo, P., "Circularly-Towed Lumped Mass Cable Model Validation from Experimental Data," AIAA Paper 2006-6817, Aug. 2006.
[27] Williams, P., Lansdorp, B., and Ockels, W., "Modeling and Control of a Kite on a Variable Length Flexible Inelastic Tether," AIAA Paper 2007-6705, Aug. 2007.
[28] Williams, P., Lansdorp, B., and Ockels, W., "Optimal Cross-Wind Towing and Power Generation with Tethered Kites," AIAA Paper 2007-6823, Aug. 2007.
[29] Elnagar, J., Kazemi, M. A., and Razzaghi, M., "The Pseudospectral Legendre Method for Discretizing Optimal Control Problems," *IEEE Transactions on Automatic Control*, Vol. 40, No. 10, 1995, pp. 1793–1796.
doi:10.1109/9.467672
[30] Ross, I. M., and Fahroo, F., "Legendre Pseudospectral Approximations of Optimal Control Problems," *Lecture Notes in Control and Information Sciences*, Vol. 295, Springer–Verlag, New York, 2004, pp. 327–342.
[31] Ross, I. M., Gong, Q., and Sekhavat, P., "Low-Thrust, High Accuracy Trajectory Optimization," *Journal of Guidance, Control, and Dynamics*, Vol. 30, No. 4, 2007, pp. 921–933.
doi:10.2514/1.23181
[32] Josselyn, S., and Ross, I. M., "Rapid Verification Method for the Trajectory Optimization of Reentry Vehicles," *Journal of Guidance, Control, and Dynamics*, Vol. 26, No. 3, 2003, pp. 505–508.